PAPER

# Transglutaminase-mediated assembly of multi-enzyme pathway onto TMV brush surfaces for synthesis of bacterial autoinducer-2

Biofabrication

PAPER

# Transglutaminase-mediated assembly of multi-enzyme pathway onto TMV brush surfaces for synthesis of bacterial autoinducer-2

Narendranath Bhokisham[1,2], Yi Liu[2], Adam D Brown[2,3], Gregory F Payne[2,4], James N Culver[2,5] and William E Bentley[2,3,4,6]

[1] Biological Sciences Graduate Program - College of Computer, Mathematical and Natural Sciences, 4066 Campus Drive, University of Maryland, College Park, MD 20742, United States of America
[2] Institute of Bioscience and Biotechnology Research, College Park, 5115 Plant Sciences Building, University of Maryland, College Park, MD 20742, United States of America
[3] Fischell Department of Bioengineering, A. James Clark Hall, University of Maryland, College Park, MD 20742, United States of America
[4] Robert E. Fischell Institute for Biomedical Devices, Room 5102, A. James Clark Hall, University of Maryland, College Park, 20742, United States of America
[5] Department of Plant Science and Landscape Architecture, 2102 Plant Sciences Building College Park, MD 20742, United States of America
[6] Author to whom any correspondence should be addressed.

**E-mail:** bentley@umd.edu

**RECEIVED**
21 October 2019

**REVISED**
12 May 2020

**ACCEPTED FOR PUBLICATION**
19 June 2020

**PUBLISHED**
28 July 2020

**Keywords:** virus like particles, transglutaminase, 3D interface materials, self-assembly, quorum sensing, enzyme cascade, biofabrication

Supplementary material for this article is available online

## Abstract

Bioelectronic microdevices, with spatially arranged biosynthetic machinery, can be programmed to convert raw materials to high-value products in a controlled manner. Generic methods for biofunctionalization that enable precise control over biocomponent assembly at the nano and meso scales are necessary to diversify the range and capabilities of these systems. Here, we used tobacco mosaic virus (TMV) derived virus like particles (VLPs) as 3D interfacial scaffolds for the assembly of biosynthetic enzymes onto gold electrodes. The TMV capsids are aligned in a vertical brush configuration by cysteine modifications to the capsid protein and by taking advantage of the well-known gold/cysteine affinity. This alignment enables high surface density and biosynthetic enzyme-enzyme proximity. Enzymes are covalently tethered to the capsid protein of TMV by the N- and C-terminal addition of lysine-rich assembly domains which react with surface exposed glutamine residues on the capsid surfaces; the lysine/glutamine linkages are mediated by a microbial transglutaminase (mTG). We demonstrate flexible mTG-mediated assembly of a three-enzyme biosynthetic pathway that converts S-adenosylmethionine (SAM) to autoinducer-2 (AI-2), a bacterial signal molecule that mediates quorum sensing behavior. We propose that our VLP and mTG based fabrication approach will help in the modular assembly of biological components onto microelectronic devices and that these will find utility in many applications including sensing and lab on chip devices.

## 1. Introduction

We previously demonstrated the electrically programmed assembly and control of a two-enzyme biochemical pathway that synthesizes a biological signaling molecule, autoinducer-2 (AI-2), on a biohybrid device [1]. The pathway consisted of a single multidomain fusion protein that was engineered with affinity ligands facilitating assembly onto a polysaccharide interface [2]. In this work, we demonstrate a more generic and modular assembly methodology that integrates individual pathway enzymes on a high-density 3D scaffold material that, in turn, is assembled onto a gold microelectronic surface. We are particularly attracted by the potential for electronic control of biological systems [1, 3] and we believe that methods that enable both electronic assembly and control will enable a variety of new functions, including programmed alteration of the microbiome of the gastrointestinal tract [4, 5], among others. Owing to their convenient ability to interact with both electronic and biologic systems [6, 7],

we expect that redox modalities will serve as principal vectors for information transfer in these emerging devices [8, 9]. That is, redox reactions that are activated by electrodes can effectively transfer information to biological systems; equally importantly, biological systems can generate redox based information that can be readily interpreted electrochemically [9–11]. Thus, by building smart interfaces that enable bidirectional information transfer across the communication modalities of biology and electronics [12–14], tremendous advances from electrogenetics to programmable biological function are envisioned [1, 3, 15, 16]. To facilitate these developments, it is important that the devices are manufactured using hybrid methodologies that accommodate and embrace the labile nature of biological components.

Electrical stimuli-responsive assembly [17–19] and self-assembly methodologies [20–22] complement the ever-expanding nanoscale capabilities of electronics with incorporation of biological components on the electrode, thus enabling complex bioassembly [10, 23–25], control [1, 3], as well as direct analytical measurement of performance [8, 26, 27]. Recently, virus and virus derived materials have been engineered as scaffold materials for facile assembly of biocomponents onto devices [28, 29] and specifically, they have been used for conjugating enzymes for biosensing applications in a biodevice context [30–32]. Cys residue engineered Tobacco mosaic virus like particles (TMV-VLPs), in particular, form self-assembled monolayers in a high density vertically aligned brush format that can be used in sensing [27, 33] and battery applications [34–37].

Here, we employed a 3D self-assembled monolayer comprised of TMV-VLPs as a base material interface and demonstrate the sequential assembly of a three-enzyme metabolic pathway onto the electrode surfaces. There are no printers or stamping equipment needed for assembly, rather we exploit the well-known cysteine/gold affinity and the use of transglutaminase for coupling proteins to each other via engineered lysine and glutamine tags [23, 38, 39]. This concept, illustrated in Scheme 1, exploits a TMV-based virus particle engineered with a Cys residue at the N terminus and two glutamine residues at the C terminus of each capsid subunit. First, TMV particle assembly onto gold surfaces is enabled by the cysteine-modification [33]. Then, capsid surface-exposed glutamine residues enable covalent conjugation of enzymes that are engineered with lysine-rich residues (referred as K tags) at their C- or N-termini via microbial transglutaminase-based conjugation chemistry [38–40]. Analogously, glutamine rich residues (referred as Q tags) at either the C- or N-terminus enables mTG-mediated coupling to K tag modified enzymes. Here, combinations of these modifications enabled the assembly of a three enzyme synthesis cascade comprising of i) trans-aconitate methyl transferase (Tam), ii) S-adenosylhomocysteine nucleosidase (Pfs) and iii) S-ribosylhomocysteine lyase (LuxS) that sequentially convert S-adenosylmethionine (SAM) to a quorum-sensing mediating bacterial signaling molecule, autoinducer-2 (AI-2). That is, SAM is converted to S-adenosylhomocysteine (SAH) and a methyl group acceptor by Tam, then the SAH is converted to S-ribosylhomocysteine (SRH) and adenosine by Pfs, and then, SRH is converted to homocysteine and 4,5-dihydroxy 2,3 pentanedione (DPD or also referred to as autoinducer-2 (AI-2), mediator of quorum sensing in bacteria) by LuxS. Notably, the terminal synthase, LuxS, exists *in vivo* as a homodimer with zinc at the active site, which, in turn is at the dimer interface. The methodologies described here enable LuxS activity while immobilized, presumably in monomeric form, but at a lower turnover number. Importantly, we found (i) the sequence by which these enzymes were best linked to the capsids and (ii) the sequence by which the capsid/particle assembly was placed onto gold that best guided the generation of AI-2 from SAM. That is, because the assembly methodology is generic and modular, comprised of proteins engineered with Q and K-tags and cysteine-engineered TMV capsids, the components can be assembled in ways that optimize overall function. There is great flexibility for designing protein complexes, including functional metabolic pathways, that are to be assembled in high density onto gold electrodes.

## 2. Materials and methods

### 2.1. Strains and plasmids

All the plasmids and strains used in this study are listed in Supplementary Table 1. We performed all cloning and transformations as per standard protocols [41]. Primers (Integrated DNA Technologies) used for construction of plasmid constructs are summarized in Supplementary Table 2. We used pET28 a-TMV1Cys plasmid [33] as template for TMV-VLP coat protein engineering.

### 2.2. Pathway enzymes expression and purification

To express pathway enzymes, we built plasmid constructs and transformed them into appropriate *E. coli* hosts (Supplementary Table 1). We grew bacteria in LB media (Sigma-Aldrich) and induced at $OD_{600}$ of 0.4 with 1 mM IPTG (Sigma Aldrich). After growth for 4 h at 30 °C, we centrifuged the cells and resuspended in 15 ml of 10 mM phosphate buffered saline (PBS), pH 7.4 (Sigma-Aldrich). To lyse the cells, we performed sonication for 15 min and centrifuged again at 20 000 g for 20 mins to remove soluble proteins. To purify His-tagged enzymes, we performed immobilized metal ion chromatography via HiTrap columns (GE Healthcare) and later dialyzed the purified enzymes with PBS and stored at −20 °C. We selectively removed His tags of all $_{K}Enzyme_{K}$'s

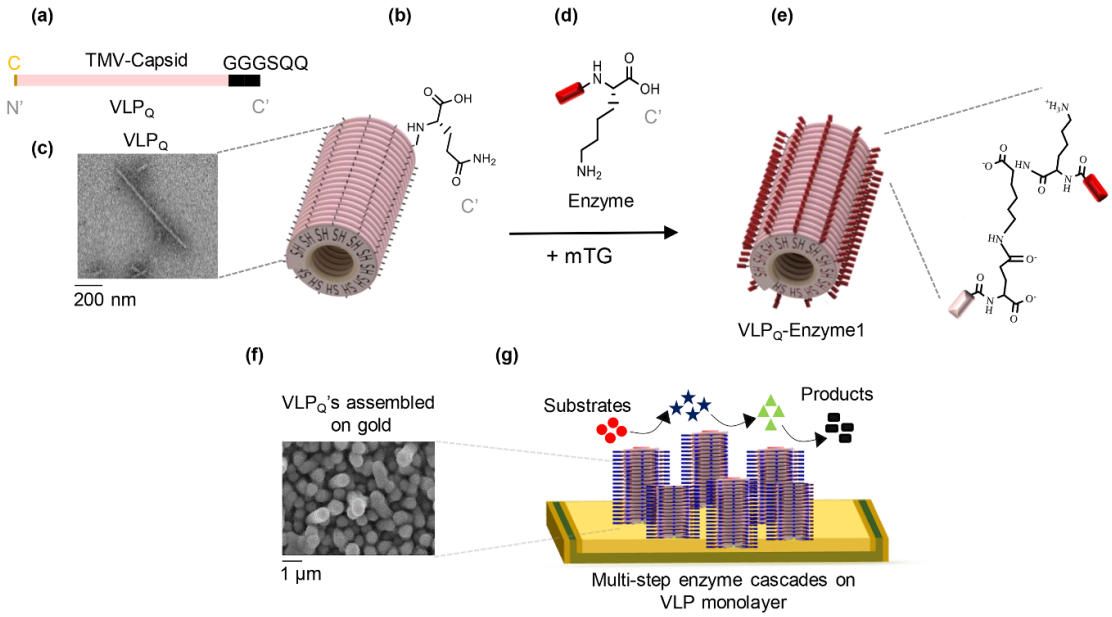


**Scheme 1. Engineered tobacco mosaic viruses-virus like particles (TMV-VLP) as 3D scaffolds for enzyme cascade assembly onto microchips** (**a**) TMV capsid subunits engineered with 1 Cys residue at N termini and 2 Q residues at C termini. (**b**) Engineered capsid subunits self assembled into virus like particles (VLP$_Q$) with Cys residues exposed at the 3′ end of the particle and Q residues on the outer surface. (**c**) TEM image indicating fully assembled TMV-VLPs with engineered capsid subunits (VLP$_Q$); Scale: 200 nm. (**d**) Enzymes engineered with K tags at C termini or N termini or both are conjugated to VLP$_Q$ using microbial transglutaminase (mTG). (**e**) mTG mediated conjugation with transpeptide bond formation between engineered K and Q residues. (**f**) SEM image of VLP$_Q$ assembled onto surface of gold coated microchip; Scale: 1 µm. (**g**) Multi-step enzyme cascade is assembled onto the surface of a gold microchip using VLP$_Q$ as 3D scaffolds using the mTG-based conjugation chemistry.

(enzymes engineered with K tags at both the N and the C termini) used in this study by incubation with enterokinase overnight at 4 °C as per manufacturer's specifications (EK-Away, Invitrogen). Enzymes were stored for further use at −20 °C.

### 2.3. Tobacco mosaic virus-like particle (TMV-VLP) purification

We transformed plasmids encoding TMV capsid proteins into the BL21 CodonPlus strain (Agilent) for expression. We grew cells in LB media to $OD_{600}$ of 0.4 and induced with 1 mM IPTG. After induction for 24 h at 30 C, we pelleted the cultures and resuspended in 2.5 ml of Bugbuster (EMD Millipore), 2 $\mu$l of 1 M DTT (Sigma) and 1 $\mu$l of Lysonase (EMD Millipore). We incubated at RT for 45 min with gentle shaking. After incubation, we added 10% (v/v) of chloroform to each tube, vortexed and centrifuged at 4000 rpm for 20 min. We separated the supernatant and pelleted in an ultracentrifuge at 30 000 rpm for 60 min at 4 C. Later, we re-suspended the pellets in 2 ml of 0.1 M phosphate buffer, pH 7 by gently shaking the pellets for overnight at 4 C and transferred into 10%–40% sucrose gradients in 0.1 M phosphate buffer, pH 7 and centrifuged at 22 500 rpm for 60 min at 4 C (supplementary figure 1 (available at stacks.iop.org/BF/12/045017/mmedia)). We extracted the TMV-VLPs in the gradients and centrifuged again at 30 000 rpm for 60 min. Finally, we re-dissolved the VLP pellets in 0.1 M phosphate buffer, pH 7 for later use.

### 2.4. Electron microscopy of TMV-VLP

Transmission electron microscopy: We adsorbed the VLP samples onto Formvar-coated Ni TEM grids by floating the grid on 5–10 $\mu$l droplets containing the sample arrayed on Parafilm™. We then washed the grids thrice by placing on 50 $\mu$l droplets of 0.1 M Tris pH 7 for 5 mins each time. We then stained the grids by placing them on a 5 $\mu$l droplet of 2% uranyl acetate (UA) for 1 min and later removed the UA by wicking with filter paper and imaged the samples using a Zeiss transmission electron microscope (TEM) at 80 kV. Scanning electron microscopy: We prepared palladium stock solution containing 0.01 g $Na_2PdCl_4$ in 1.5 ml methanol and nickel stock solution containing 0.6 g $NiCl_2$ hexahydrate, 0.45 g glycine, 1.5 g sodium tetraborate and 0.77 g dimethylamine borane complex in 25 ml $H_2O$. We covered 5 $mm^2$ chips with 25 $\mu$g of VLP$_Q$ in solution and incubated for overnight at 4 C. Following overnight incubation with VLPs, we washed the chips with 30 ml of 0.1 M phosphate buffer, pH 7 and submerged in a 30X dilution of palladium stock solution for 30 min at RT. After 30 min incubation, we washed the chips with PBS and submerged the chips in 2X dilution of nickel stock solution. After 30 min, we washed the chips again and dried for 5 mins and used for scanning electron microscopy. In results, we show the TEM and SEM images of the VLP$_Q$ particles and as brush configured onto gold. In previous work we have shown with electron microscopy how TMV particles retain their shape when coated with metal [33] and

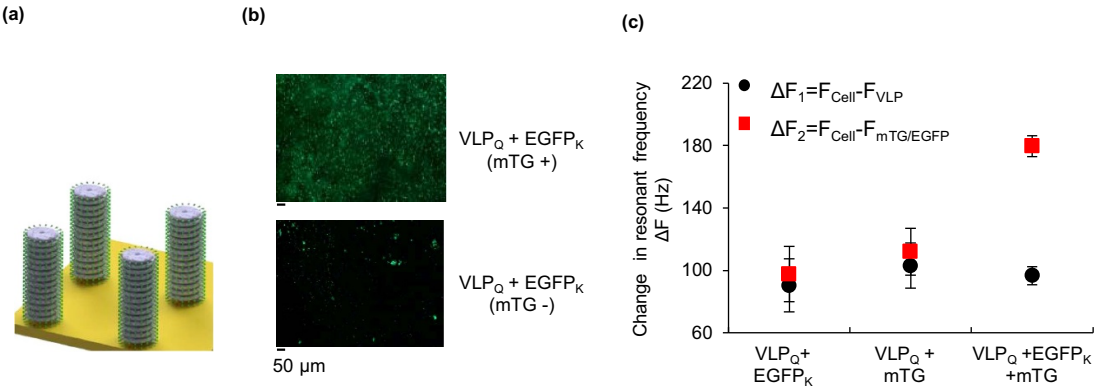


**Figure 1. Qualitative and quantitative evidence for protein assembly onto VLP via mTG mediated conjugation.** **(a)** Assembly of $EGFP_K$ (EGFP engineered with K tag at C termini) onto $VLP_Q$ monolayer assembled on chips using microbial transglutaminase (mTG) and engineered tags. **(b)** Fluorescence microscopy images of $EGFP_K$ conjugated to $VLP_Q$; Scale: 50 $\mu$m. **(c)** Quantitative analysis was performed using a Quartz Crystal Microbalance (QCM) indicating changes in resonant frequency due to conjugation of $EGFP_K$ to $VLP_Q$ in the presence of mTG. $VLP_Q$ were first assembled onto QCM chips; the frequency shifts are attributed to the assembly of $VLP_Q$s (indicated by black circles ($\Delta F_1$)). Later, $EGFP_K$ was conjugated to $VLP_Q$ via mTG and the associated frequency shifts are indicated by red squares ($\Delta F_2$). Error bars indicate standard deviation across three independent sensors used for each condition, n = 3.

glucose oxidase[31]. In other work (unpublished), we have shown full length antibody conjugation to TMV VLPs. Here, electron micrographs are not shown for each assembly, instead we have focused on the preservation of enzymatic activity when bound.

### 2.5. Preparation of gold chips

Prior to any experiment, all gold coated chips (Platypus Technologies) were first immersed in piranha solution [3:1 mixture of Sulfuric Acid ($H_2SO_4$) with Hydrogen Peroxide ($H_2O_2$)] for 5 mins, rinsed with Super Q water and dried in a stream of compressed air. Post the completion of conjugation experiments, gold chips were first immersed in methanol for 15 mins and the piranha solution based cleaning step (indicated above) was repeated to clean the chips again.

### 2.6. Assembly of $VLP_Q$ monolayer

To the cleaned chips, we added 25 $\mu$g of VLPs (100 $\mu$ls in volume) onto 100 $mm^2$ gold chips and incubated the chips at 4 °C overnight. After incubation, we performed a wash step by gently flowing 30 ml of 0.1 M phosphate buffer, pH 7 onto the gold chips to remove unbound VLPs and used for further experiments. Unless mentioned otherwise, we refer to the use of 30 ml of 0.1 M phosphate buffer, pH 7 as the wash step to remove unbound proteins in all our experiments.

### 2.7. Conjugation of EGFP onto VLPs for fluorescence microscopy

We first assembled the $VLP_Q$ monolayer onto the gold chips as described above. Later, we blocked the chips with 100 $\mu$l of 5% bovine serum albumin (BSA) solution and incubated at 37 °C for 60 min. After incubation, we washed the chips again (as indicated in the methods above) and added 7.5 $\mu$M $EGFP_K$ and 10 $\mu$M microbial transglutaminase (mTG) in a combined total volume of 20 $\mu$ls onto $VLP_Q$ layer on gold chips. All the solutions were mixed well and spread to cover the entire area of the 100 $mm^2$ and chips were incubated at RT for 60 min. After incubation, we washed the chips again and used further for fluorescence microscopy.

### 2.8. Conjugation of enzymes onto VLPs and measurement of enzyme activity

After the assembly of $VLP_Q$ monolayer onto gold chips (area: 100 $mm^2$) as detailed above, to conjugate any enzyme, we used the varying concentration of suitably tagged enzyme (for example a K tagged LuxS when conjugated to $VLP_Q$ monolayers) and mTG for conjugation. We then incubated the reaction for 60–120 min (depending on each experiment) at RT and then washed the chips with 0.1 M phosphate buffer, pH 7 as detailed above. Later to test the enzyme activity of immobilized enzyme, we provided appropriate substrate and other enzymes required to complete the reaction. For example, when LuxS is immobilized, to mediate conversion of SAH to HCY, we provided 1 mM SAH and 3 $\mu$M of soluble Pfs in 10 mM phosphate buffered saline, pH 7.4 (PBS) to the VLP-LuxS monolayers. After incubation at 37 °C for 1–2 h (depending on the experiment), we measured HCY via Ellman's assay.

### 2.9. Enzymatic conversion of S-adenosylmethionine (SAM) and S-adenosylhomocysteine (SAH) to homocysteine (HCY)

To mediate conversion of SAM to HCY, we added all three enzymes in the cascade, Tam, Pfs, and LuxS (either in soluble or in immobilized form) and added 1 mM SAM along with 20 mM trans-aconitic acid (TAA) in 0.4 M HEPES buffer, pH 7.5 and incubated at 37 °C for 60 min. After incubation, we

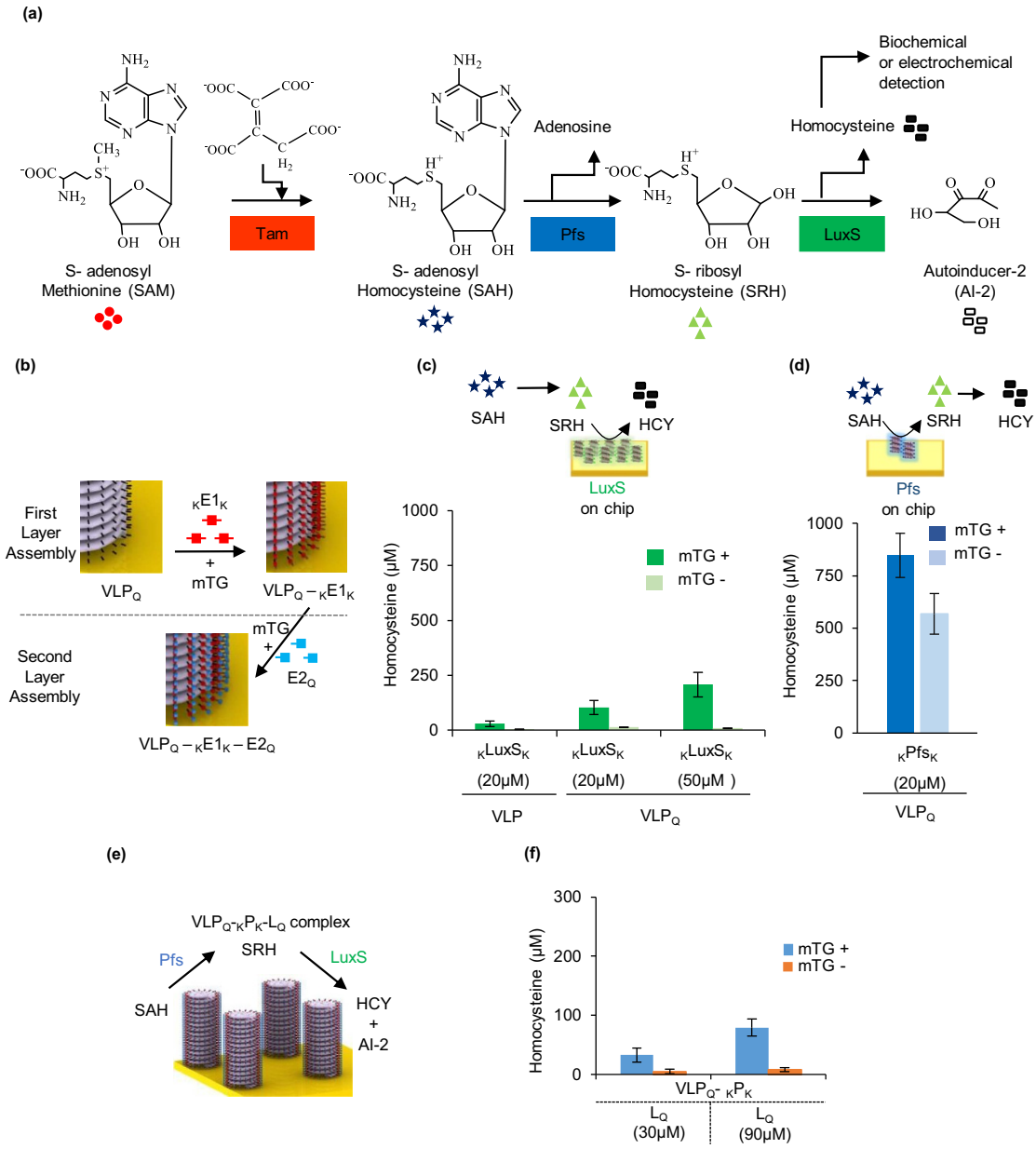


**Figure 2. Assembly of enzymes involved in conversion of S-adenosylmethionine (SAM) to homocysteine (HCY) onto microchips.** (**a**) Three enzyme cascade for conversion of S-adenosylmethionine (SAM) to Homocysteine (HCY). Tam converts SAM to S-adenosylhomocysteine (SAH). Pfs converts SAH to S-ribosylhomocysteine (SRH). LuxS converts SRH to homocysteine (HCY) and autoinducer-2 (AI-2). (**b**) Assembly of two-enzyme cascade onto $VLP_Q$. The first layer is comprised of enzyme 1 engineered with K tags at both N and C termini ($_KE1_K$) and second layer is comprised of enzyme 2 engineered with Q tag at C termini ($E2_Q$). Pfs (**c**) and LuxS (**d**) engineered with K tags at both the N and the C termini is conjugated separately to $VLP_Q$ assembled on the surface of microchips. These immobilized enzymes are provided with 1 mM SAH and the other remaining enzymes for HCY generation provided at non-rate limiting conditions (3 $\mu$M of each enzyme). Reactions are incubated at 37 C for 2 h and the amounts of HCY generated is quantified using Ellman's assay, n = 3. (**e**) Assembly of $VLP_Q$-$_KP_K$-$L_Q$ complex with the first layer comprised of $_KP_K$ and a second layer comprised of $L_Q$. (**f**) Homocysteine yields obtained from $VLP_Q$-$_KP_K$-$L_Q$ complexes. Enzyme complex is incubated with 1 mM SAH for 2 h at 37 C and the amounts of HCY generated is quantified using Ellman's assay, n = 3.

measured the amounts of HCY generated using both the Ellman's assay as described in Fernandes *et al* [2] and an electrochemical assay using cyclic voltammetry as shown in supplementary figure 2.

## 3. Results

### 3.1. Protein conjugation to VLP monolayers via mTG

Having previously demonstrated Cys-engineered TMV brush assembly onto gold [27, 33, 36, 37], we show in figure 1 the analogous assembly of a Q engineered TMV (denoted $VLP_Q$) that can be decorated with K tagged proteins [38–40]. That is, in figure 1(a), we depict the covalent coupling of GFP engineered with K tags. We added 7.5 $\mu$M $EGFP_K$ and 10 $\mu$M microbial transglutaminase (mTG) onto $VLP_Q$ that had been pre-assembled onto gold chips and incubated at RT for 60 min. Later, we washed the chips (refer methods) and imaged using fluorescence microscopy (figure 1(b)). Widely distributed GFP

fluorescence was observed while analogous control experiments without mTG show almost no binding after the wash step. Next, to quantify the amount of protein conjugated to the monolayer, we used quartz microbalance (QCM). We measured changes in the resonant frequency ($\Delta F$) of each individual gold coated quartz crystal chip (ICM, Oklahoma, USA) at each stage of the assembly process to characterize assembly. We assembled $VLP_Q$ monolayer on the gold coated area (area: 20 $mm^2$) of the quartz crystal chip by incubating 25 $\mu$g of VLPs for overnight at 4°C. After incubation, we removed the excess $VLP_Q$ by washing with Super Q water (note: we used super Q water instead of 0.1 M phosphate buffer for all the washing steps concerning QCM), then we vacuum dried (at RT for 60 min) and measured the VLP-chip resonant frequency ($F_{VLP}$). We next added 7.5 $\mu$M $EGFP_K$ and 10 $\mu$M microbial transglutaminase (mTG) and incubated at RT for 60 min. Post incubation, we washed, and vacuum dried the chips again and remeasured the frequency ($F_{mTG/EGFP}$). As expected, control experiments without mTG or $EGFP_K$ showed negligible frequency change. Using Saurbrey's equation [42], we correlated the changes in resonant frequency ($\Delta F_1$ and $\Delta F_2$) to the amount of material assembled on the sensor at each step. We estimated that ~100 ng of $VLP_Q$ was assembled on the chip surface (20 $mm^2$) and ~1.15 ng of $EGFP_K$ was conjugated per 1 ng of $VLP_Q$ on the chip, indicating ~47% coverage of $VLP_Q$ surface with $EGFP_K$. Both conjugation controls had ~0.1ng of proteins assembled per 1 ng of $VLP_Q$ indicating a 10-fold difference between mTG mediated conjugation and nonspecific binding of EGFP on sensors. These results confirm that EGFP engineered with C-terminal lysines can be conjugated to $VLP_Q$ monolayers assembled onto gold using mTG-mediated conjugation chemistry [39].

### 3.2. Sequential assembly of metabolic pathway onto VLP-scaffolds via mTG

In figure 2, we show the sequential assembly of pathway enzymes comprising of Tam, Pfs and LuxS onto $VLP_Q$ monolayers for conversion of SAM to AI-2 (figure 2(a)). Importantly, AI-2 has been shown to influence the microbiome of the human GI tract [43], its electronically controlled synthesis and delivery presents an interesting way to potentially modulate the GI microflora in a programmed manner. In our potential application, AI-2 synthesis can be indirectly quantified by electronically measuring the stoichiometrically co-produced produced homocysteine through cyclic voltammetry (supplementary figure 2) or the Ellman's calorimetric assay [44].

For simplicity, we first conjugated VLPs with each of the enzymes to create VLP-enzyme conjugates and then added various amounts of enzyme-VLP conjugates onto the gold chip to ascertain their loading and activity when assembled onto the gold chips (supplementary figure 3). Interestingly, Pfs (mediating the reaction from SAH to SRH) was active as conjugated and then deposited. In general, however, we found limited conversion of these aggregates post mTG addition as they were typically unstable and relatively inactive. Hence, we pursued an alternative assembly strategy. That is, in earlier work, we showed how lysine and glutamine tagged Pfs and LuxS could be sequentially coupled onto polystyrene beads [39]. Similarly, here we next explored the assembly of a two-enzyme pathway comprising Pfs and LuxS onto $VLP_Q$ scaffolds that had been pre-assembled onto gold coated microchips. We individually immobilized each enzyme in the pathway onto the $VLP_Q$ monolayer and determined their relative enzyme activities when immobilized. We used Pfs and LuxS enzymes engineered with K tags at both the N and the C termini (denoted ${}_KP_K$ and ${}_KL_K$, respectively) and conjugated them to the $VLP_Q$ monolayers (figure 2(b)). In all experiments, we first assembled the $VLP_Q$ monolayers onto the gold surfaces as indicated in methods by incubating 25 $\mu$g of $VLP_Q$ onto gold chips (area: 100 $mm^2$) and performed blocking and washing steps as detailed in methods.

To test conjugation of each enzyme, we provided substrates and enzymes of the upstream and downstream reactions in soluble form and in excess to reconstruct the entire pathway *in vitro*; we then measured the final products, AI-2 and HCY after specified reaction times. In figure 2(c), we conjugated LuxS, the last enzyme in the three-enzyme cascade onto $VLP_Q$ monolayers. We added 20 $\mu$M and 50 $\mu$M concentrations of $L_K$ along with 10 $\mu$M of mTG for conjugation and incubated for 60 min at RT. As controls, we performed the same reactions without mTG. After incubation, we washed the chips with phosphate buffer (Methods) and provided 1 mM SAH and 3 $\mu$M of soluble Pfs to the VLP-LuxS monolayers. After incubation at 37 °C for 2 h, we measured HCY and results show that increased concentrations of LuxS correlated with increased HCY yielding 20% conversion from SAH to HCY overall in the 2 hr incubation time. These data indicate that at the concentrations and conditions tested, LuxS was the rate-limiting factor [39]. We note that controls without mTG resulted in negligible HCY. As an added control, we used a VLP monolayer lacking the engineered glutamines at the C termini of the capsid proteins (denoted VLP instead of $VLP_Q$). Interestingly, there was some HCY generation (above that of the mTG(-) control) suggesting minor amounts of LuxS conjugation to native VLP glutamines or otherwise nonspecific binding to the TMV capsid.

In an exactly analogous manner, we conjugated 20 $\mu$M of $P_K$ to the $VLP_Q$ monolayers (figure 2(d)). After washing, we added 1 mM SAH and LuxS (provided in excess, 3 $\mu$M) in PBS. After 2 h of incubation at 37 °C, we measured HCY. Results indicated 85% conversion of SAH to HCY indicating that

$P_K$ had higher activity than LuxS when immobilized, assuming similar mTG binding efficiencies. Unexpectedly, we noted that conjugation controls without mTG exhibited ~65% conversion. While not investigated further, we suspect this was due to an appreciable level of nonspecific affinity between Pfs and the $VLP_Q$ monolayers [24]. More importantly, *in situ* assembled Pfs retained significant activity on $VLP_Q$. In additional work, we determined Km, Vmax and kcat values for immobilized enzymes (Supplementary figure 4). Results indicated that kcat was highest for Pfs. Moreover, the values calculated were within the ranges previously reported for immobilized Pfs [24]. There is no prior report on LuxS immobilization, however Km and Vmax values for soluble LuxS have been estimated and we observed a ~ 70-fold increase in Km values for LuxS, suggesting impaired substrate binding to the LuxS immobilized with VLPs. That is, our previous work to immobilize these pathway enzymes focused on Pfs, as the procedures used (e.g. tyrosinase tag [24, 45], chitosan magnetic nanoparticles [46], and antibody methods [25]) rarely showed activity for LuxS and hence were not reported. Given that LuxS exists as a homodimer in solution with residues from both subunits involved in the enzyme active sites [47], we hypothesize that conjugation of LuxS onto VLPs may have impaired its ability to form homodimers, leading to increased binding coefficients and lowered activity.

After demonstrating assembly of Pfs and even, LuxS, individually onto $VLP_Q$ monolayers, we explored assembly of a two-enzyme cascade comprising of Pfs and LuxS for the conversion of SAH to HCY [39, 40]. We intended to assemble this two enzyme cascade sequentially with the first layer consisting of Pfs engineered with a K tag at both the N and the C termini ($_KP_K$) and the second layer consisting of LuxS with a Q tag at the C terminus ($L_Q$) (figure 2(e)). We expected that lysines of one of the termini of $_KP_K$ would conjugate to the $VLP_Q$ monolayer and lysines at the other termini would be available to conjugate to the Q residues in the second enzyme $L_Q$. For the first assembly, we added 30 $\mu$M $_KP_K$ and 10 $\mu$M mTG for Pfs conjugation onto the $VLP_Q$ monolayer. After conjugation for 60 min at RT, we washed the chips (methods) and performed another round of mTG mediated conjugation with different concentrations of $L_Q$ (30 and 90 $\mu$M) at a stoichiometric ratio of 1:1 and 1:3 with Pfs in the first layer. Post assembly and washing, we next provided 1 mM SAH in PBS for 2 h at 37 °C and measured HCY, as before. Importantly, we found significant activity and also observed that the increased LuxS concentration during incubation resulted in increased HCY, again indicating LuxS as the rate limiting enzyme (figure 2(f)). We note that HCY yields obtained from conjugation of LuxS as the second enzyme layer resulted in somewhat lower HCY levels than tests with LuxS conjugated as the first layer and providing the other components in excess (figure 2(c)). Considering previously noted constraints imposed by this sequential assembly process that suggest the second enzymes are added at slightly reduced levels than the first and the rate limitation due to LuxS, we thought of assembling LuxS as the first layer and Pfs as the second layer. That said, we had also observed earlier that sandwiching LuxS between two layers reduces its enzyme activity [39] and thus, we suggest here that reduced activity results from a combination of these factors and perhaps the relative inability of LuxS to form a homodimeric structure. We have not investigated these issues any further at this time. Importantly, we were able to retain LuxS activity in this configuration, demonstrating a two enzyme cascade that retained biosynthetic activity when sequentially conjugated onto gold-assembled VLPs with LuxS as the terminal layer. We used these complexes in further studies.

In sum, results in figure 2 demonstrate that engineered AI-2 synthesis enzymes, Pfs and LuxS, individually assembled onto $VLP_Q$ chips retained their activities with kinetic parameters of Pfs substantially higher than LuxS, when immobilized. The enzyme cascade was assembled in a sequential format that enabled the conversion of SAH to AI-2. The apparent reduction in specific yield that occurred with two enzymes linked to the $VLP_Q$ was exactly analogous to our earlier work with polystyrene beads [39], revealing potential limitations relative to the number of enzymes that can be strung together using the mTG-mediated coupling to engineered lysine and glutamine tags.

### 3.3. Assembly of a three-enzyme cascade onto VLP monolayer

Having achieved success in assembling a two enzyme cascade onto surface assembled VLPs, we sought to expand the system to the full three-enzyme pathway. That is, a three-enzyme cascade consisting of Tam, Pfs and LuxS grafted onto $VLP_Q$ monolayers would enable conversion of S-adenosylmethionine (SAM) fully to homocysteine (HCY) and AI-2 (figure 3(a)). Thus, we engineered and purified *E. coli* trans-aconitate methyl transferase (Tam) with K tags at both the N and C termini (referred to as $_KT_K$). With other pathway enzymes (Pfs and LuxS) provided in excess (3 $\mu$M), we first determined the quantity of soluble enzyme, $_KT_K$, to be active (Supplementary figure 5) and hence conjugated $_KT_K$ onto the $VLP_Q$ monolayer and measured enzyme activities when bound. We provided 1 mM SAM (Tam substrate) with Pfs and LuxS (each in excess and soluble, 3 $\mu$M) and incubated for 2 h at 37 °C. We measured HCY indicating ~30% conversion (figure 3(b)). As anticipated, controls without mTG resulted in minimal HCY. We also measured Km and Vmax values for Tam when conjugated to the VLP monolayer (Supplementary figure 4) and found it to be better than LuxS, while Pfs was still the best performing enzyme in the cascade.

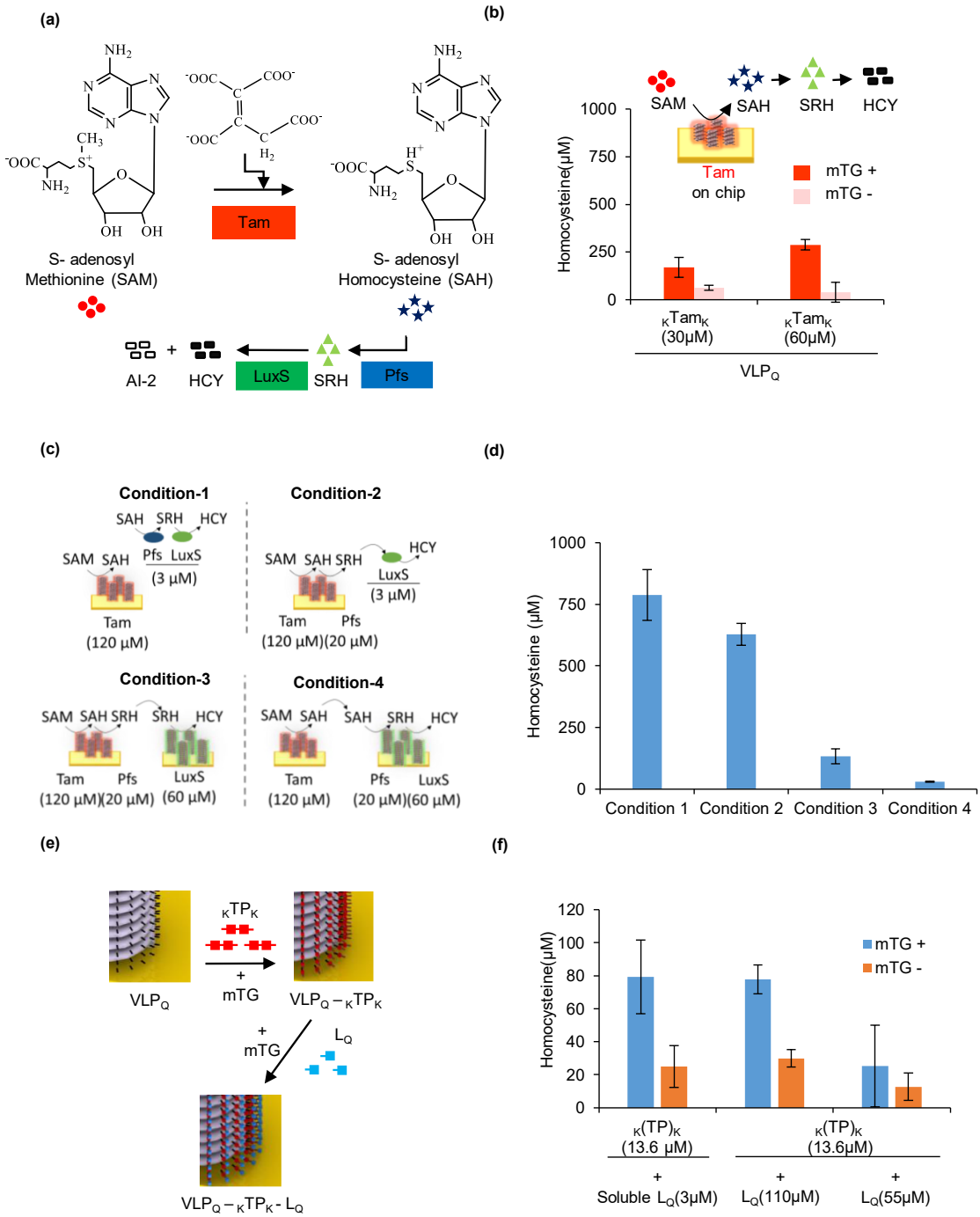


**Figure 3. mTG mediated sequential assembly of three enzyme cascade onto gold chips.** (**a**) Three enzyme cascade for conversion of S-adenosylmethionine (SAM) to homocysteine (HCY). Trans-aconitate methyltransferase (Tam) converts SAM to SAH. Then, Pfs and LuxS converts SAH to HCY and AI-2. (**b**) Tam engineered with K tags at both the N and the C termini is conjugated separately to $VLP_Q$ assembled on the surface of microchips. These immobilized enzymes are provided with 1 mM SAM and the other remaining enzymes (Pfs and LuxS) for HCY generation provided at non-rate limiting conditions (3 $\mu$M of each enzyme). Reactions are incubated at 37 C for 2 h and the amounts of HCY generated are quantified using Ellman's assay, n = 3. (**c**) Scheme depicts various conditions used for the assembly of three enzymes in one or two-chip configurations. Condition 1 had just one chip with Tam immobilized on the VLP monolayer. Condition 2 had 1 chip with both Tam and Pfs. Condition 3 had two chips, with Tam and Pfs on the first chip and LuxS on the second chip. Condition 4 had two chips, with Tam on the first chip and Pfs and LuxS on the second chip. Other enzymes required for HCY generation are provided in solution at a non-rate limiting concentrations (3 $\mu$M of each enzyme) (**d**) HCY yields obtained via Ellman's assay from all 4 conditions after incubation with 1 mM SAM for 2 h at 37 °C. n = 3. (**e**) Assembly of $VLP_Q$-$_\kappa TP_\kappa$-$L_Q$ complex with the first layer comprised of an Tam-Pfs fusion enzyme engineered with K tags at both N and C termini ($_\kappa TP_\kappa$) and a second layer comprised of LuxS engineered with Q tag at the C termini ($L_Q$). (**f**) Biochemical data from $VLP_Q$-$_\kappa TP_\kappa$-$L_Q$ complex. Enzyme complex is reacted with 1 mM SAM and incubated for 2 h and HCY is measured using Ellman's assay, n = 3.

Since there are no prior reports of Tam functionalization onto solid supports, we were not able to compare activities of Tam enzyme immobilized onto VLP scaffolds.

We had originally intended to assemble all the three enzymes Tam, Pfs and LuxS onto $VLP_Q$ in a sequential fashion. However, since there had been a reduction in enzyme activity with increased layers (figure 2(f)), we took advantage of the modular nature of the process and split the assembly of the three-enzyme cascade into two chips of equal sizes (100 $mm^2$) and placed them side-by-side. That is, this also demonstrates the flexibility of deploying enzymes onto VLPs that are preassembled onto gold surfaces. To test this concept, we used four conditions with different enzyme arrangements in each (figure 3(c)). In condition 1, we had 120 $\mu$M of $_KT_K$ conjugated to $VLP_Q$ monolayer on gold chips (referred as $VLP_{Q\text{-}K}T_K$) and provided the other two enzymes, Pfs and LuxS (3 $\mu$M each), in solution. In condition 2, we had 120 $\mu$M of $_KT_K$ conjugated to $VLP_Q$ monolayer on gold chips as the first layer of enzymes and then added a second layer in which $P_Q$ (20 $\mu$M) was conjugated to $_KT_K$ (referred as $VLP_{Q\text{-}K}T_K\text{-}P_Q$) with a stoichiometric ratio of 1:0.2 between Tam and Pfs. We also provided LuxS (3 $\mu$M) in solution. In condition 3, we had $VLP_{Q\text{-}K}T_K\text{-}P_Q$ on the first chip, as in condition 2, but then added $L_K$ (60 $\mu$M) to the $VLP_Q$ monolayer in a second chip. Finally, in condition 4, we conjugated 120 $\mu$M of $_KT_K$ to the $VLP_Q$ monolayer for chip 1 and then used $VLP_{Q\text{-}K}P_K\text{-}L_Q$ in chip 2 that was built with a stoichiometric ratio of 1:3 between Pfs and LuxS (20 $\mu$M of Pfs and 60 $\mu$M of LuxS). In all these conditions, we provided 1 mM SAM as substrate, incubated at 37 °C for 2 h and measured the HCY yields using the Ellman's assay. Results in figure 3(d) revealed that condition 1 with $_KT_K$ conjugated to $VLP_Q$ monolayer had highest HCY yields with ~75% conversion of SAM to HCY. Condition 2, containing Tam and Pfs in a single chip had marginally lower yields than in condition 1 with ~60% conversion. HCY yields from conditions 3 and 4 with LuxS in a second chip were not surprisingly higher than 20%, again indicating a limitation from bound LuxS in the overall cascade.

To partially offset reduced conjugation that accompanied a sequential or multi-layer approach and the intrinsic reduction in LuxS activity when bound, we also adopted a genetic fusion strategy that combines Tam and Pfs into a single protein (denoted TP) and conjugated it to the $VLP_Q$ monolayer. That is, in previous studies, we found it efficacious to create two-enzyme fusions first *in vitro* using genetic engineering [2], followed by the consecutive fabrication on solid surfaces [1]. Since Tam and Pfs were relatively more robust than LuxS, we genetically engineered and expressed a fusion protein containing equimolar Tam and Pfs connected by an 8aa flexible linker. We assembled this fusion protein as the first layer onto $VLP_Q$. To enable conjugation, we engineered TP with K tag at both the N and C termini (denoted $_KTP_K$, figure 3(e)). To facilitate purification, we also added a $His_6$ tag and an enterokinase (EK) cleavage site at the N terminus of $_KTP_K$ (denoted His-EKsite-$_KTP_K$). We conjugated varying concentrations of His-EKsite-$_KTP_K$ onto VLPs and later incubated the conjugated enzymes with 1 mM SAM and 3 $\mu$M soluble LuxS for 2 h at 37 C. With increased concentration of His-EKsite-$_KTP_K$ fusion during incubation, we observed increased yield (Supplementary figure 6). These results demonstrated that both the Tam and Pfs enzymes as engineered with assembly tags remained active, including as conjugated to each other and with $VLP_Q$.

Additionally, we removed the His-EKsite purification tag from the fusion enzyme via enterokinase-mediated cleavage (see Methods) to expose the engineered lysines at both the N and C termini (referred as $_KTP_K$). We conjugated the same quantity of $_KTP_K$ to the $VLP_Q$ monolayers and measured conversion. Surprisingly, the yield was nearly 4-fold lower than His-EKsite-$_KTP_K$ (Supplementary figure 7(a)) while there was minimal difference in enzyme activity between the two fusion enzymes in solution (Supplementary figure 7(b)). Our results suggest that the reduction in enzyme activity of $_KTP_K$ upon immobilization may be due an exposed N terminal lysine that might have been used for conjugation onto the $VLP_Q$ monolayer resulting in possible obstruction of the active site of Tam in the Tam-Pfs enzyme fusion. That is, the engineered lysines are further from the enzyme and their conjugation may not influence the activity when compared to lysines more proximal to the remainder of the enzyme. We note, however, this is purely conjecture and more experiments would be required to verify this hypothesis.

Having shown the flexibility in enzyme pathway engineering via localization of functionalized chips, we wanted to further demonstrate activity from VLPs decorated with the full set of three enzymes. In figure 3(f), we added $_KTP_K$ (devoid of EK site) as the first layer and followed with $L_Q$ in the second. Specifically, we added 13.6 $\mu$M of $_KTP_K$ along with 30 $\mu$M mTG onto $VLP_Q$. After incubation for 2 h at RT and washing, we added 55 $\mu$M and 110 $\mu$M of $L_Q$ (at a stoichiometric ratio of 1:4 and 1:8 with $_KTP_K$ in the first layer) for another round of conjugation. Post incubation and wash steps, we incubated the assembled enzyme cascade with 1 mM SAM for 2 h at 37 C. Controls without mTG were also tested. Interestingly, the HCY yields indicated that the 110 µM condition with LuxS added as the second layer produced equivalent amounts of HCY as the single layer $VLP_{Q\text{-}K}TP_K$ complex with LuxS provided in solution (figure 3(f)). While HCY yields of around 80 $\mu$M were lower than the earlier experiments (figure 2), they were in line with expectations from identical conditions where equivalent amount of TP fusion enzyme is conjugated to VLPs with LuxS provided in solution (Supplementary figure 6). That is, in this work we found that LuxS when conjugated as the second assembled unit was as reactive as that provided in solution. We note, however, the amount of LuxS provided for conjugation

was ~30 fold higher than that used to obtain similar conversion levels when provided in solution, reiterating some of the challenges experienced by conjugating enzymes that typically require dimerization. This observation notwithstanding, the flexibility and ease by which enzymatic assembly can be utilized is noteworthy.

In sum, we successfully demonstrated a transglutaminase-mediated conjugation approach that enables the assembly of a three-enzyme reaction cascade onto virus like particles that had been preassembled onto gold surfaces through their N-terminal Cys residues. Importantly, because the methodology developed here makes use of assembly tags engineered onto the respective protein termini, there is great flexibility in the order of assembly that can result in a highly reactive system. That is, we found the enzymes exhibited varied activity when conjugated or otherwise tagged with assembly ligands but were able to develop 2-chip systems or 3-enzyme 1-chip systems that had equivalent overall activity.

## 4. Conclusions

We have developed a methodology for rapid and simple self-assembly of enzymatic pathways that are displayed onto 3D VLP scaffolds in ways that preserves their functions and enables microsystem synthesis of small molecules. The overall system makes use of the enhanced surface area enabled by the vertically aligned brush morphology when TMV VLPs are assembled onto gold electrodes through engineered Cys residues. In our system, the TMV VLP needs an assembly-enabling glutamine residue at its C-terminus so that covalent attachment of lysine-tagged proteins can be facilitated by transglutaminase.

In the specific case of AI-2 synthases Tam, Pfs, and LuxS, we found Pfs had the highest intrinsic activity (i.e. its turnover number was greatest), followed by Tam and LuxS (supplementary figure 3) and, in addition, both Tam and LuxS had reduced enzyme activities when immobilized. Hence during cascade fabrication, the stoichiometries of these enzymes were adjusted to account for altered enzyme activities during immobilization. Importantly, this is easily accomplished owing to the concentration and surface area driven enzymatic reactions that enable protein assembly. While conceptually simple and at first glance, completely generic, we did find that the efficiency of conjugation (as indicated in figure 3) decreased as increasing layers were added. This was partially offset by: (i) using a fusion construct for the first two enzymes; (ii) using adjacent electrodes in a 2-chip strategy, and (iii) by the addition of a third enzyme to the previously assembled enzyme fusion. That is, when we genetically fused Tam and Pfs together and assembled it as the first layer and then added LuxS, the least efficient enzyme in the second layer, results were quite positive. We had observed earlier that the reversal of the order, with LuxS as the first layer, was far less effective. In this arrangement, we obtained our best result for conversion of SAM to HCY and AI-2 and removed the LuxS limitation in the immobilized three enzyme cascade (figure 4(f)).

The novelty of this approach is that we utilized bio-based materials and techniques for hierarchical assembly of interfacial materials and synthetic cascades directly onto electronic surfaces. In addition to several conjugation chemistries that have been genetically engineered into $VLP_Q$ for conjugation of cargoes, we have added mTG-mediated conjugation chemistry for protein assembly onto $VLP_Q$. This utilizes facile and rapid mTG chemistry that enables multiple steps and preserves nanoscale spatial resolution. The significance of the work is that the process of integrating biological components with electronics is simplified due to the self-assembly of the interfacial material (VLPs) and the subsequent enzymatic-coupling of engineered enzymes. That is, we believe 3D scaffolds used in combination with convenient enzyme-mediated conjugation chemistry enables biologically benign integration of more complex systems at electrode interfaces. This, in turn, enables the use of redox-mediated information transfer [7] such as the detection of various biochemicals using electrochemical means [26, 11] or even the electronic control of biological function [1, 3]. TMV-$VLP_Q$ are used here as the 3D scaffolds; they can be used as interface materials in biosensors and biosynthesis devices. Such synthetic enzyme cascades, when assembled onto the surfaces of microelectronic chips, could be developed into fully functioning biosensors for the various pathway substrates (e.g. SAM and SAH). Moreover, we envision that AI-2 synthesis systems could be incorporated into microbiome altering devices, including electronically-controlled ingestible capsules, wherein controlled delivery of microbial signaling molecules may alter the microbiota composition and potentially, function [43, 48, 49]. The assembly of enzyme pathways and complexes onto microelectronic devices holds great promise in a variety of applications.

## Acknowledgments

N-B designed and performed the experiments, A-D-B and Y-L assisted in performing the experiments, G-F-P and J-N-C provided technical inputs and reviewed the manuscripts, N-B and W-E-B authored the manuscripts. We would also like thank DTRA (HDTRA1-13-0037), NSF (DMREF #1435957, ECCS#1807604, CBET#1805274, CBET#1841506), the National Institutes of Health (R21EB024102), and Agilent, Inc., for their generous support.

## ORCID iDs

Gregory F Payne https://orcid.org/0000-0001-6638-9459
William E Bentley https://orcid.org/0000-0002-4855-7866

## References

[1] Gordonov T, Kim E, Cheng Y, Ben-Yoav H, Ghodssi R, Rubloff G, Yin J-J, Payne G F and Bentley W E 2014 Electronic modulation of biochemical signal generation *Nat. Nano* **9** 605–10
[2] Fernandes R, Roy V, Wu H-C and Bentley W E 2010 Engineered biological nanofactories trigger quorum sensing response in targeted bacteria *Nat. Nano* **5** 213–7
[3] Tschirhart T, *et al* 2017 Electronic control of gene expression and cell behaviour in Escherichia coli through redox signalling *Nat. Commun.* **8** 14030
[4] Mimee M *et al* 2018 An ingestible bacterial-electronic system to monitor gastrointestinal health *Science* **360** 915–8
[5] Banis G E, Beardslee L A, Stine J M, Sathyam R M and Ghodssi R 2019 Gastrointestinal targeted sampling and sensing via embedded packaging of integrated capsule system *J. Microelectromech. Syst.* **28** 219–25
[6] Kang M, Kim E, Li J Y, Bentley W E and Payne G F 2018 Redox: electron-based approach to bio-device molecular communication *IEEE Int. Work Sign P.* pp 1–5
[7] Kim E *et al* 2019 Redox is a global biodevice information processing modality *Proc. IEEE* **107** 1402–24
[8] Liu Y *et al* 2017 Using a redox modality to connect synthetic biology to electronics: hydrogel-based chemo-electro signal transduction for molecular communication *Adv. Healthcare Mater.* **6** 1600908
[9] Liu Y, *et al* 2017 Connecting biology to electronics: molecular communication via redox modality *Adv. Healthcare Mater.* **6** 1700789
[10] Yan K, Liu Y, Guan Y, Bhokisham N, Tsao C Y, Kim E, Shi X-W, Wang Q, Bentley W E and Payne G F 2018 Catechol-chitosan redox capacitor for added amplification in electrochemical immunoanalysis *Colloids Surf.* B **169** 470–7
[11] VanArsdale E, Tsao C Y, Liu Y, Chen C Y, Payne G F and Bentley W E 2019 Redox-based synthetic biology enables electrochemical detection of the herbicides dicamba and roundup via rewired escherichia coli *ACS Sens.* **4** 1180–4
[12] Offenhäusser A and Rinaldi R 2009 *Nanobioelectronics - For Electronics, Biology, and Medicine Introduction* A Offenhausser and R Rinaldi ed (Berlin: Springer) pp 1–3
[13] Willner I and Katz E ed 2005 Bioelectronics: from theory to applications (New York: Wiley) p 1–475
[14] Simon D T, Gabrielsson E O, Tybrandt K and Berggren M 2016 Organic bioelectronics: bridging the signaling gap between biology and technology *Chem. Rev.* **116** 13009–41
[15] Luo X, Lewandowski A T, Yi H, Payne G F, Ghodssi R, Bentley W E and Rubloff G W 2008 Programmable assembly of a metabolic pathway enzyme in a pre-packaged reusable bioMEMS device *Lab. Chip.* **8** 420–30
[16] Luo X, Wu H-C, Tsao C-Y, Cheng Y, Betz J, Payne G F, Rubloff G W and Bentley W E 2012 Biofabrication of stratified biofilm mimics for observation and control of bacterial signaling *Biomaterials* **33** 5136–43
[17] Yi H, Wu L-Q, Bentley W E, Ghodssi R, Rubloff G W, Culver J N and Payne G F 2005 Biofabrication with chitosan *Biomacromolecules* **6** 2881–94
[18] Liu Y *et al* 2012 Biofabricating multifunctional soft matter with enzymes and stimuli-responsive materials *Adv. Funct. Mater.* **22** 3004–12
[19] Li J *et al* 2019 Electrobiofabrication: electrically based fabrication with biologically derived materials *Biofabrication* **11** 032002
[20] Boncheva M, Bruzewicz D A and Whitesides G M 2003 Millimeter-scale self-assembly and its applications *Pure Appl. Chem.* **75** 621–30
[21] Braun E and Keren K 2004 From DNA to transistors *Adv. Phys.* **53** 441–96
[22] Keren K, Berman R S and Braun E P 2004 DNA metallization by sequence-specific localization of a reducing agent *Nano Lett.* **4** 323–6
[23] Liu Y, Wu H-C, Bhokisham N, Li J, Hong K-L, Quan D N, Tsao C-Y, Bentley W E and Payne G F 2018 Biofabricating functional soft matter using protein engineering to enable enzymatic assembly *Bioconjugate Chem.* **29** 1809–22
[24] Lewandowski A T, Bentley W E, Yi H, Rubloff G W, Payne G F and Ghodssi R 2008 Towards area-based *in vitro* metabolic engineering: assembly of pfs enzyme onto patterned microfabricated chips *Biotechnol. Progr.* **24** 1042–51
[25] Wu H-C *et al* 2009 Biofabrication of antibodies and antigens via IgG-binding domain engineered with activatable pentatyrosine pro-tag *Biotechnol. Bioeng.* **103** 231–40
[26] Tschirhart T, Zhou X Y, Ueda H, Tsao C-Y, Kim E, Payne G F and Bentley W E 2016 Electrochemical measurement of the β-galactosidase reporter from live cells: a comparison to the miller assay *ACS Synth. Biol.* **5** 28–35
[27] Zang F, Gerasopoulos K, Fan X Z, Brown A D, Culver J N and Ghodssi R 2014 An electrochemical sensor for selective TNT sensing based on Tobacco mosaic virus-like particle binding agents *Chem. Commun.* **50** 12977–80
[28] Wen A M and Steinmetz N F 2016 Design of virus-based nanomaterials for medicine, biotechnology, and energy *Chem. Soc. Rev.* **45** 4074–126
[29] Culver J N, Brown A D, Zang F, Gnerlich M, Gerasopoulos K and Ghodssi R 2015 Plant virus directed fabrication of nanoscale materials and devices *Virology* **479** 200–12
[30] Aljabali A A A, Barclay J E, Steinmetz N F, Lomonossoff G P and Evans D J 2012 Controlled immobilisation of active enzymes on the cowpea mosaic virus capsid *Nanoscale* **4** 5640–5
[31] Koch C, Wabbel K, Eber F J, Krolla-Sidenstein P, Azucena C, Gliemann H, Eiben S, Geiger F and Wege C 2015 Modified TMV particles as beneficial scaffolds to present sensor enzymes *Front. Plant Sci.* **6** 1137
[32] Bäcker M, Koch C, Eiben S, Geiger F, Eber F, Gliemann H, Poghossian A, Wege C and Schöning M J 2016 A new class of biosensors based on tobacco mosaic virus and coat proteins as enzyme nanocarrier *Procedia Eng.* **168** 618–21
[33] Brown A D, Naves L, Wang X, Ghodssi R and Culver J N 2013 Carboxylate-directed in vivo assembly of virus-like nanorods and tubes for the display of functional peptides and residues *Biomacromolecules* **14** 3123–9
[34] Liu Y, Xu Y, Zhu Y, Culver J N, Lundgren C A, Xu K and Wang C 2013 Tin-coated viral nanoforests as sodium-ion battery anodes *ACS Nano* **7** 3627–34
[35] Lee Y J, Lee Y, Oh D, Chen T, Ceder G and Belcher A M 2010 Biologically activated noble metal alloys at the nanoscale: for lithium ion battery anodes *Nano Lett.* **10** 2433–40
[36] Royston E, Ghosh A, Kofinas P, Harris M T and Culver J N 2008 Self-assembly of virus-structured high surface area nanomaterials and their application as battery electrodes *Langmuir* **24** 906–12
[37] Konstantinos G, Matthew M, Elizabeth R, James N C and Reza G 2008 Nanostructured nickel electrodes using the tobacco mosaic virus for microbattery applications *J. Micromech. Microeng.* **18** 104003
[38] Bhokisham N, Liu Y, Pakhchanian H, Payne G F and Bentley W E 2017 A facile two-step enzymatic approach for conjugating proteins to polysaccharide chitosan at an electrode interface *Cell. Mol. Bioeng.* **10** 134–42
[39] Bhokisham N, Pakhchanian H, Quan D, Tschirhart T, Tsao C Y, Payne G F and Bentley W E 2016 Modular construction of multi-subunit protein complexes using engineered tags and microbial transglutaminase *Metab. Eng.* **38** 1–9
[40] Bhokisham N, Pakhchanian H, Quan D, Tschirhart T, Tsao C-Y, Payne G F and Bentley W E 2016 Data on

biochemical fluxes generated from biofabricated enzyme complexes assembled through engineered tags and microbial transglutaminase *Data Brief.* **8** 1031–5
[41] Sambrook J 2001 *Molecular Cloning: A Laboratory Manual*, editors J Sambrook, D W Russell and L Cold Spring Harbor (New York: Cold Spring Harbor Laboratory)
[42] Sauerbrey G 1959 Verwendung von schwingquarzen zur wägung dünner schichten und zur mikrowägung *Z. Phys.* **155** 206–22
[43] Thompson Jessica A, Oliveira Rita A, Djukovic A, Ubeda C and Xavier Karina B 2015 Manipulation of the quorum sensing signal AI-2 affects the antibiotic-treated gut microbiota *Cell Rep.* **10** 1861–71
[44] Wang L, Li J, March J C, Valdes J J and Bentley W E 2005 luxS-dependent gene regulation in escherichia coli k-12 revealed by genomic expression profiling *J. Bacteriol.* **187** 8350–60
[45] Lewandowski A T, Small D A, Chen T, Payne G F and Bentley W E 2006 Tyrosine-based 'activatable pro-tag': enzyme-catalyzed protein capture and release *Biotechnol. Bioeng.* **93** 1207–15
[46] Fernandes R and Bentley W E 2009 AI-2 biosynthesis module in a magnetic nanofactory alters bacterial response via localized synthesis and delivery *Biotechnol. Bioeng.* **102** 390–9
[47] Hilgers M T and Ludwig M L 2001 Crystal structure of the quorum-sensing protein LuxS reveals a catalytic metal site *Proc. Nal. Acad. Sci.* **98** 11169–74
[48] Xavier K B 2018 Bacterial interspecies quorum sensing in the mammalian gut microbiota *C R Biol.* **341** 300
[49] Thompson J A, Oliveira R A and Xavier K B 2016 Chemical conversations in the gut microbiota *Gut Microbes* **7** 163–70